

LETTERS

Thermal conductivity of single-crystalline AIN

To cite this article: Robert Rounds et al 2018 Appl. Phys. Express 11 071001

View the article online for updates and enhancements.

Related content

- Preparation of a Freestanding AIN Substrate from a Thick AIN Layer Grown by Hydride Vapor Phase Epitaxy on a Bulk AIN Substrate Prepared by Physical Vapor

<u>Transport</u> Yoshinao Kumagai, Yuki Kubota, Toru Nagashima et al.

- PVT growth of AIN single crystals with the diameter from nano- to centi-meter level H Wu, R Zheng, Y Guo et al.
- Preparation of Bulk AIN Seeds by Spontaneous Nucleation of Freestanding Crystals Carsten Hartmann, Juergen Wollweber,

Andrea Dittmar et al.

Thermal conductivity of single-crystalline AIN



Robert Rounds¹, Biplab Sarkar¹, Andrew Klump¹, Carsten Hartmann³, Toru Nagashima⁴, Ronny Kirste^{1,2}, Alexander Franke¹, Matthias Bickermann³, Yoshinao Kumagai⁵, Zlatko Sitar^{1,2}, and Ramón Collazo¹

Received April 20, 2018; accepted May 27, 2018; published online June 11, 2018

The thermal conductivity of AIN single crystals grown by physical vapor transport (PVT) and hydride vapor phase epitaxy (HVPE) was measured in the range of 30 to $325 \, \text{K}$ by the 3ω method. The measured room-temperature thermal conductivity ranged from 268 to $374 \, \text{W} \, \text{m}^{-1} \, \text{K}^{-1}$. Higher thermal conductivity correlated with higher transparency at 265 nm and lower total impurity levels. © 2018 The Japan Society of Applied Physics

luminum nitride (AlN) is a wide-bandgap material with uses in next-generation UV light-emitting diodes, laser diodes, and power semiconductor devices. 1-4) Future devices based on AlN are expected to operate at high power densities owing to the 15 MV cm⁻¹ breakdown field. 5-7) High power densities will directly affect thermal management approaches, making the thermal conductivity of AlN a crucial device design parameter. Prior work has shown that the concentration of point defects incorporated during AlN crystal growth significantly affects the thermal conductivity of AlN. 8-10) Carbon impurities create an additional problem because they introduce an absorption band at 265 nm, ¹¹⁾ precluding the intended use in some UV-C optoelectronic devices. The introduction of additional oxygen and silicon restores UV transparency by negating the presence of carbon, ^{12,13)} but this is expected to decrease thermal conductivity proportionally because of the increase in the rate of phonon-point defect scattering. In the present work, we study AlN crystals containing different point defects and examine the effects of defects on thermal conductivity and the connection to UV transparency.

In order to observe the relationship between UV transparency and thermal conductivity, AlN single crystals with absorption coefficients at 265 nm in the density range of 7 to ~1000 cm⁻¹ were selected. Expected dislocation densities were <10⁴ cm⁻² for all crystals on the basis of typical results from samples fabricated by PVT and HVPE AlN growth processes. ^{12,14–16} The PVT AlN samples were prepared in schematically similar reactors at IKZ and HexaTech, the details of which are described elsewhere. ^{17,18} Sample thickness ranged from 200 μm in the HVPE AlN and lowest absorbing PVT AlN sample to 2 mm in the highly absorbing PVT AlN. Table I lists the results of secondary ion mass spectrometry (SIMS) for the studied samples. Table II lists the absorption coefficients at 265 nm, the thermal conductivities at room temperature, and the thicknesses of the samples.

The wafers were patterned for 3ω measurements by photolithography and metallized using a UHV electron beam metal evaporation system. The metallization layers were rendered with liftoff in NMP, after which the samples were placed in a vacuum cryostat for testing. Details on the 3ω setup are described elsewhere. ²⁰⁾ Measuring the dependence of thermal conductivity on temperature reveals the relative contributions of different phonon scattering mechanisms. For the studied temperature range, the dominant phonon scattering mechanisms are primarily three phonon/Umklapp processes and

Table I. Impurity concentrations determined by SIMS (atoms cm⁻³). Values for PVT AlN 5 are estimates based on average impurity concentrations found in UV-absorbing PVT AlN substrates. ^{11,13,15,19})

Sample	С	О	Si	Total
HVPE AIN	4.59×10^{16}	3.08×10^{17}	2.80×10^{17}	6.34×10^{17}
PVT AlN 1	1.68×10^{18}	6.94×10^{18}	6.92×10^{17}	9.31×10^{18}
PVT AlN 2	2.09×10^{18}	8.13×10^{18}	2.28×10^{18}	1.25×10^{19}
PVT AlN 3	9.90×10^{18}	2.00×10^{18}	1.30×10^{19}	2.49×10^{19}
PVT AlN 4	1.10×10^{19}	2.80×10^{17}	1.10×10^{19}	2.23×10^{19}
PVT AlN 5	$\sim 2.5 \times 10^{19}$	$\sim 8.6 \times 10^{18}$	$\sim 9.4 \times 10^{18}$	\sim 4.3 × 10 ¹⁹

Table II. Absorption coefficients at 265 nm, room-temperature thermal conductivities, and sample thicknesses.

AlN Sample	α at 265 nm (cm ⁻¹)	κ at 295 K (W m ⁻¹ K ⁻¹)	Thickness (µm)
HVPE AIN	7	341 ± 6	204
PVT AlN 1a)	21	374 ± 9	200
PVT AlN 2a)	53	343 ± 7	340
PVT AlN 3b)	70	339 ± 7	550
PVT AlN 4 ^{b)}	277	301 ± 5	470
PVT AlN 5 ^{b)}	>1000	268 ± 5	2000

a) Grown at IKZ.

scattering by point defects, such as vacancies and impurities. The incorporation of point defects significantly affects thermal conductivity at lower temperatures as seen in Fig. 1.

The technologically important room-temperature thermal conductivity of the PVT AlN samples ranges from 268 to 374 W m⁻¹ K⁻¹, significantly higher than results in prior literature. ^{9,21)} The convergence of the curves at higher temperatures indicates a dominating 3 phonon/Umklapp scattering rate relative to the rate of point defect scattering, a trait clearly illustrated in other crystalline materials. ^{22–25)} In order to put the measured results in context relative to the expected behavior of a pure crystal of AlN containing no point defects, a simulated curve using the Debye approximation of thermal conductivity is provided in Fig. 2.

The model curve generally matches the data at temperatures above 200 K and compares well with prior modelling for pure AlN, but the results at low temperature significantly diverge from the simulation. Prior literature from studies of other crystal systems demonstrates a similar lack of low-temperature behavioral resemblance between model curves and

¹Department of Materials Science and Engineering, North Carolina State University, Raleigh, NC 27695, U.S.A.

²Adroit Materials, Inc., Cary, NC 27518, U.S.A.

³Leibniz Institute for Crystal Growth (IKZ), 12489 Berlin, Germany

⁴Tsukuba Research Laboratories, Tokuyama Corporation, Tsukuba, Ibaraki 300-4247, Japan

⁵Department of Applied Chemistry, Tokyo University of Agriculture and Technology, Koganei, Tokyo 184-8588, Japan

b) Grown at HexaTech, Inc.

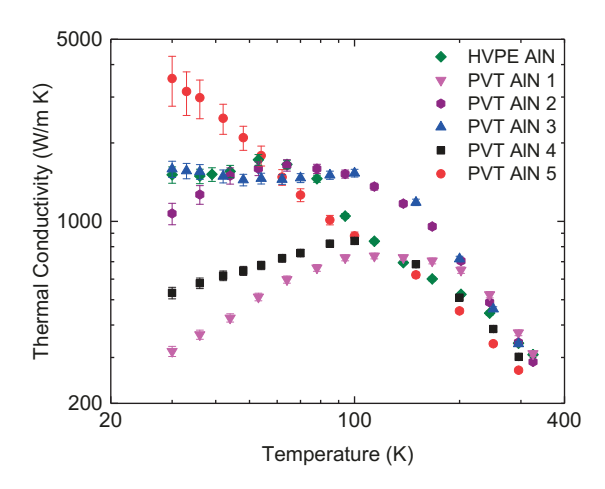


Fig. 1. Thermal conductivity of AlN as a function of temperature.

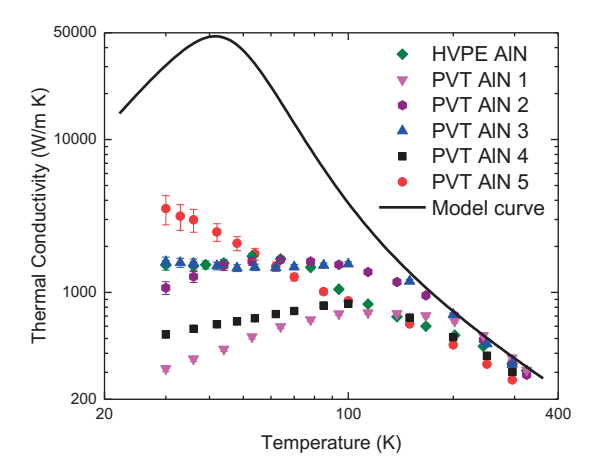


Fig. 2. Experimental results and simulated curve for pure AlN, as given by the Debye approximation. The calculated curve neglects phonon scattering contributions from normal processes, uses a sound velocity of 7094 m/s, a Debye temperature (θ_D) of 967 K, a characteristic length of 2 mm, and a Grüneisen parameter (γ) of 2. Sound velocity and θ_D were determined using the elastic constants for AlN, ²⁶ leaving γ as the only adjustable parameter.

measured results.^{27–30)} The presence of this same discrepancy between the ideal curve and the experimental data for all the AlN samples studied indicates substantial phonon resonance scattering, an effect described in previous work. ^{27–30)} The absence of alignment between the measured results at low temperature and the $\sim T^3$ dependence shown between 20–30 K in the model curve also indicates that thermal conductivity is not yet within the boundary scattering regime and therefore is still under the influence of point defects for all the crystals. The measured thermal conductivity for PVT AlN 2 and 3 coincides to that at around 100 K, indicating a similar influence of Umklapp scattering. PVT AlN 1 shows a maximum of 736 W m⁻¹ K⁻¹ at 114 K and has the highest thermal conductivity at temperatures above 240 K, but this sample exhibits the lowest thermal conductivity for all temperatures below 140 K. The thermal conductivity for PVT AlN 2 exhibits a clear maximum of 1641 W m⁻¹ K⁻¹ between 60 and 70 K and demonstrates the smoothest temperature-dependent behavior. However, the apparent shift towards the boundary scattering regime occurs at a higher temperature than expected, as the boundary scattering length should be approximately equal between samples PVT AlN 2, 3, and 4.

Accordingly, the thermal conductivity results of PVT AlN 2 are most likely still dominated by point defect scattering below 60 K. PVT AlN 4 shows lower transparency and its thermal conductivity reaches a maximum of ~840 W m⁻¹ K⁻¹ near 100 K, below which the thermal conductivity decrease is nearly linear with the log of temperature. Because of the lower thermal conductivity in PVT AlN 4 than in PVT AlN 3, one would expect to find a higher point defect density in the former, but this is not observed in Table I. The curve for PVT AlN 5 shows a significant influence of point defects, as indicated by its lower thermal conductivity between room temperature and 100 K. Nonetheless, this sample shows less sensitivity to low-temperature phonon resonances than the other samples, as it has the highest thermal conductivity below 50 K. The HVPE AlN curve shows some overlap with the curve for PVT AlN 4, but reaches a maximum thermal conductivity of 1723 W m⁻¹ K⁻¹ near 50 K. While the HVPE AlN sample has the fewest impurities, it lags behind PVT AlN 2 and 3 in thermal conductivity between room temperature and 80 K. PVT AlN 4 has 3×10^{18} fewer impurities than PVT AlN 3, but has poorer thermal conductivity over the entire temperature range. PVT AlN 1 has the lowest impurity concentration among the PVT AlN samples, yet it shows the lowest thermal conductivity below 140 K. Finally, PVT AlN 2 has half the impurities of PVT AlN 3, but thermal conductivity results from the two samples coincide between room temperature and 100 K.

While these results partially contradict the expectation of a simple inverse relationship between thermal conductivity and impurity concentration, prior thermal conductivity studies of other single-crystal materials have yielded the following results. (a) The dimensional arrangement of incorporated impurities within the lattice significantly affects the location of the curve maximum with respect to temperature. (b) Curve distortion from phonon resonances positively correlates with impurity concentration, sometimes at levels as low as $10^{16} \, \mathrm{cm}^{-3}.^{27-29)}$ (c) The interplay between impurity types may also affect curve behavior if their interaction changes the associated phonon scattering cross section within the crystal lattice. (d) The concentration of vacancies as well as heavy elements from the PVT crucible materials was not quantified.

The distribution of point defects within the crystals of the present work and the degree to which they interact are unknown, but the findings of prior work indicate that the reduction or compensation of carbon is necessary to reduce absorption at 265 nm. 11,13,32,33) Thermal conductivity above 200 K appears to scale directly with the concentration of carbon in the PVT samples as well as relate inversely to the absorption coefficient at 265 nm. Compensation of the presence of carbon in the PVT AlN samples may partially explain their high UV transparency, but the influence of the carbon complex formation on thermal conductivity via the modification of the impurity-phonon scattering cross sections cannot be determined within the present work. Finally, the distortion seen in the curve for HVPE AIN indicates that phonon resonances are still significantly active, even with impurity concentrations two orders of magnitude lower than those in the PVT AlN samples.

In conclusion, thermal conductivity was measured by the 3ω method for AlN single crystals with varying point defect concentrations in the range of 30 to 325 K. UV-transparent

PVT-grown AlN showed comparable thermal conductivity to that of HVPE AlN at room temperature. Curve distortion was evident in all samples but PVT AlN 1 and was attributed to the phonon resonances caused by point defects. Comparison of measured results against an ideal model curve for pure AlN showed significant behavioral departures in the temperature dependence of the experimental data with respect to anticipated behavior, once again suggesting active phonon resonances. Room-temperature thermal conductivity values ranged from 268 to 374 W m⁻¹ K⁻¹, the latter being the highest reported room-temperature thermal conductivity of AlN. Thermal conductivity curves converged at higher temperatures and nearly coincided at room temperature with values around 340 W m⁻¹ K⁻¹. SIMS results showed that the total impurity concentration was on the order of 10¹⁹ cm⁻³ in the PVT crystals and $10^{17}\,\mathrm{cm^{-3}}$ in the HVPE crystal, but contrary to expectation, thermal conductivity did not always follow an inverse relationship with impurity concentration. Thermal conductivity between room temperature and 200 K was directly related to carbon concentration and UV transparency in the PVT AlN crystals. The discrepancy between the experimental results, the model curve, and the traditional understanding of the influence of point defects on thermal conductivity indicate either a more complicated relationship than the simple case of dispersed and noninteracting point defects or the presence of other point defects that were not measured, such as vacancies or heavy elements from the surrounding crucible used in PVT AlN growth.³⁴⁾

Acknowledgments The authors acknowledge partial financial support from ARL (W56KGU-15-C-0052, W56KGU-14-C-0046), NSF (ECCS-1508854, ECCS-1610992, DMR-1508191, ECCS-1653383), ARO (W911NF-15-2-0068, W911NF-16-C-0101), and the German BMBF through WideBaSe (03WKBT05A) and Advanced UV for Life (03ZZ0112A). HVPE AlN growth at Tokyo University of Agriculture and Technology was partially supported by the Japan Society for the Promotion of Science (JSPS) Grant-in-Aid for Scientific Research (B) No. 15H03555.

- B. Raghothamachar, R. Dalmau, B. Moody, S. Craft, R. Schlesser, J. Q. Xie, R. Collazo, M. Dudley, and Z. Sitar, Mater. Sci. Forum 717–720, 1287 (2012).
- 2) T. Wunderer, C. L. Chua, J. E. Northrup, Z. Yang, N. M. Johnson, M. Kneissl, G. A. Garrett, H. Shen, M. Wraback, B. Moody, H. S. Craft, R. Schlesser, R. F. Dalmau, and Z. Sitar, Phys. Status Solidi C 9, 822 (2012).
- R. Collazo, S. Mita, J. Xie, A. Rice, J. Tweedie, R. Dalmau, and Z. Sitar, Phys. Status Solidi C 8, 2031 (2011).
- 4) J. Y. Tsao, S. Chowdhury, M. A. Hollis, D. Jena, N. M. Johnson, K. A. Jones, R. J. Kaplar, S. Rajan, C. G. Van de Walle, E. Bellotti, C. L. Chua, R. Collazo, M. E. Coltrin, J. A. Cooper, K. R. Evans, S. Graham, T. A. Grotjohn, E. R. Heller, M. Higashiwaki, M. S. Islam, P. W. Juodawlkis, M. A. Khan, A. D. Koehler, J. H. Leach, U. K. Mishra, R. J. Nemanich, R. C. N. Pilawa-Podgurski, J. B. Shealy, Z. Sitar, M. J. Tadjer, A. F. Witulski, M. Wraback, and J. A. Simmons, Adv. Electron. Mater. 4, 1600501 (2018).

- 5) T. L. Chu, J. Electrochem. Soc. 122, 995 (1975).
- 6) T. Kinoshita, T. Nagashima, T. Obata, S. Takashima, R. Yamamoto, R. Togashi, Y. Kumagai, R. Schlesser, R. Collazo, A. Koukitu, and Z. Sitar, Appl. Phys. Express 8, 061003 (2015).
- 7) J. Xie, S. Mia, R. Dalmau, R. Collazo, A. Rice, J. Tweedie, and Z. Sitar, Phys. Status Solidi C 8, 2407 (2011).
- R. Rounds, B. Sarkar, D. Alden, Q. Guo, A. Klump, C. Hartmann, T. Nagashima, R. Kirste, A. Franke, M. Bickermann, Y. Kumagai, Z. Sitar, and R. Collazo, J. Appl. Phys. 123, 185107 (2018).
- G. A. Slack, R. A. Tanzilli, R. O. Pohl, and J. W. Vandersande, J. Phys. Chem. Solids 48, 641 (1987).
- G. A. Slack, L. J. Schowalter, D. Morelli, and J. A. Freitas, J. Cryst. Growth 246, 287 (2002).
- 11) R. Collazo, J. Xie, B. E. Gaddy, Z. Bryan, R. Kirste, M. Hoffmann, R. Dalmau, B. Moody, Y. Kumagai, T. Nagashima, Y. Kubota, T. Kinoshita, A. Koukitu, D. L. Irving, and Z. Sitar, Appl. Phys. Lett. 100, 191914 (2012).
- C. Hartmann, J. Wollweber, S. Sintonen, A. Dittmar, L. Kirste, S. Kollowa, K. Irmscher, and M. Bickermann, CrystEngComm 18, 3488 (2016).
- 13) B. E. Gaddy, Z. Bryan, I. Bryan, J. Xie, R. Dalmau, B. Moody, Y. Kumagai, T. Nagashima, Y. Kubota, T. Kinoshita, A. Koukitu, R. Kirste, Z. Sitar, R. Collazo, and D. L. Irving, Appl. Phys. Lett. 104, 202106 (2014).
- 14) P. Lu, R. Collazo, R. F. Dalmau, G. Durkaya, N. Dietz, B. Raghothamachar, M. Dudley, and Z. Sitar, J. Cryst. Growth 312, 58 (2009).
- 15) Y. Kumagai, Y. Kubota, T. Nagashima, T. Kinoshita, R. Dalmau, R. Schlesser, B. Moody, J. Xie, H. Murakami, A. Koukitu, and Z. Sitar, Appl. Phys. Express 5, 055504 (2012).
- 16) D. Ehrentraut and Z. Sitar, MRS Bull. 34, 259 (2009).
- 17) C. Hartmann, A. Dittmar, J. Wollweber, and M. Bickermann, Semicond. Sci. Technol. 29, 084002 (2014).
- 18) R. Dalmau and Z. Sitar, in *Springer Handbook of Crystal Growth*, ed. G. Dhanaraj, K. Byrappa, V. Prasad, and M. Dudley (Springer, Berlin/Heidelberg, 2010) Chap. 24.
- 19) R. Dalmau, B. Moody, R. Schlesser, S. Mita, J. Xie, M. Feneberg, B. Neuschl, K. Thonke, R. Collazo, A. Rice, J. Tweedie, and Z. Sitar, J. Electrochem. Soc. 158, H530 (2011).
- 20) D. G. Cahill, Rev. Sci. Instrum. 61, 802 (1990).
- 21) G. A. Slack, J. Phys. Chem. Solids 34, 321 (1973).
- 22) P. D. Thacher, Phys. Rev. 156, 975 (1967).
- 23) J. E. Graebner, H. Altmann, N. M. Balzaretti, R. Campbell, H.-B. Chae, A. Degiovanni, R. Enck, A. Feldman, D. Fournier, and J. Fricke, Diamond Relat. Mater. 7, 1589 (1998).
- **24)** R. O. Carlson, G. A. Slack, and S. J. Silverman, J. Appl. Phys. **36**, 505 (1965).
- 25) G. A. Slack, Phys. Rev. 126, 427 (1962).
- D. Gerlich, S. L. Dole, and G. A. Slack, J. Phys. Chem. Solids 47, 437 (1986).
- 27) F. C. Baumann, J. P. Harrison, R. O. Pohl, and W. D. Seward, Phys. Rev. 159, 691 (1967).
- 28) J. P. Harrison, P. P. Peressini, and R. O. Pohl, Phys. Rev. 167, 856 (1968).
- V. Narayanamurti, W. D. Seward, and R. O. Pohl, Phys. Rev. 148, 481 (1966)
- 30) C. T. Walker and R. O. Pohl, Phys. Rev. 131, 1433 (1963).
- 31) R. B. Simon, J. Anaya, and M. Kuball, Appl. Phys. Lett. 105, 202105 (2014).
- 32) B. E. Gaddy, Z. Bryan, I. Bryan, R. Kirste, J. Xie, R. Dalmau, B. Moody, Y. Kumagai, T. Nagashima, Y. Kubota, T. Kinoshita, A. Koukitu, Z. Sitar, R. Collazo, and D. L. Irving, Appl. Phys. Lett. 103, 161901 (2013).
- 33) K. Irmscher, C. Hartmann, C. Guguschev, M. Pietsch, J. Wollweber, and M. Bickermann, J. Appl. Phys. 114, 123505 (2013).
- 34) F. Langhans, S. Kiefer, C. Hartmann, T. Markurt, T. Schulz, C. Guguschev, M. Naumann, S. Kollowa, A. Dittmar, J. Wollweber, and M. Bickermann, Cryst. Res. Technol. 51, 129 (2016).